https://doi.org/10.32604/zkg.2026.079278

ARTICLE

Sulfonamide-based polymer grinding aids in slag grinding and their effect on hydration performance of cement

Kai Ke[1,*], Xiang Li[1] and Yingbin Wang[2]
[1]School of Materials and Chemical Engineering, Hubei University of Technology, Wuhan, China
[2]School of Civil Engineering, Architecture and Environment, Hubei University of Technology, Wuhan, China
*Corresponding Author: Kai Ke. Email: kekai0704@163.com

Received: 18 January 2026; Accepted: 22 May 2026

ABSTRACT: Granulated blast furnace slag (GBFS) is an industrial by-product with high latent activity generated during pig iron smelting, and its unique vitreous structure results in poor grindability. Therefore, activating the latent activity and improving the grindability of GBFS have become research hotspots in the relevant field. In this study, a low-molecular-weight polymer was synthesized using 2-acrylamido-2-methylpropanesulfonic acid (AMPS), hydroxypropyl acrylate (HPA) and diethylene glycol monovinyl ether (DEGVE) as polymerizable monomers, and then compounded with polyhydric alcohol to prepare a polymer grinding aid suitable for GBFS. The effects of the polymer grinding aid on grinding efficiency and hydration properties of GBFS-blended cement paste were systematically investigated. The results showed that the particle size of GBFS ground with the polymer grinding aid was slightly coarser than that of the alkanolamine-treated sample. But the polymer grinding aid could optimize the cross-linked structure of hydration products and improve the early age and long-term strengths of GBFS-blended cement. When the dosages of initiator and chain transfer agent accounted for 1.28% and 5.14% of the total monomer mass, respectively, and the monomer molar ratio satisfied n (DEGVE):n (AMPS):n (HPA) = 1:2.65:0.5, the obtained polymer grinding aid provides a better balance between particle-size distribution optimization of GBFS and strength development of GBFS-blended cement, while the individual fineness parameters remain comparable to or slightly lower than the sample prepared with reference alkanolamine-based grinding aid. Compared with the alkanolamine-based grinding aids, the volume fractions of GBFS particles with particle sizes of 0–3 μm and above 64 μm treated by the polymer grinding aid decrease by 5.4% and 76.0%, respectively, while the volume fraction of particles with particle sizes of 32–64 μm increases by 12.2%. Correspondingly, the 7 d and 28 d compressive strengths of the GBFS-based cementitious materials are increased by 8.4% and 4.3%, respectively.

KEYWORDS: Granulated blast furnace slag; grinding aid; AMPS; polymer structural regulation; hydration performance

MATERIALS

1 Introduction

Granulated blast furnace slag (GBFS) is an industrial by-product generated during the smelting of pig iron in blast furnaces. Rapid water quenching treatment leads to the formation of the vitreous structure, with the vitreous phase content as high as 90%–95% [1]. This vitreous phase consists of two phase structures: one is a calcium-rich continuous phase, and the other is a silicon-rich discontinuous phase. The silicon-rich phase is tightly encapsulated by the calcium-rich phase, forming a typical phase-separated structure [2]. Due to the fact that the bond energy of Si-O bonds is significantly higher than that of Ca-O bonds, the calcium-rich phase is more easily crushed during the grinding process [3, 4].

Existing studies on GBFS grinding aids have mostly focused on alkanolamine-based and their modified products. Lee et al. [5] found that triethanolamine (TEA)-based composite grinding aids can effectively increase the volume fraction of slag particles in the range of 3~32 μm, but have a limited effect on improving the 28 d strength. Kim et al. and Hallet et al. [6, 7] conducted a systematic study on different types of single-component grinding aids and showed that although TEA can improve the early strength, the strength growth rate gradually decreases, resulting in a decline in the 28 d and later strength of cement. He et al. [8] investigated the effect of TEA on low-activity materials such as slag and fly ash, and the results indicated that high-calcium glassy slag is less affected by TEA. Zhao et al. [9–11] prepared glycerol phosphate through glycerol modification; its multi-polar group structure can improve the solubility of mineral phases, and the promoting effect of this grinding aid on slag

hydration is superior to that of TEA. Some studies have shown that [5, 8, 12] proposed that the addition of alkanolamine-based grinding aids can promote the hydration of aluminate minerals, thereby facilitating more sufficient hydration of silicate minerals, generating more C-S-H gel, and ultimately achieving strength improvement. Previous studies have demonstrated that [9, 10, 13, 14] pointed out that the more active groups in the grinding aid molecule, the better the grinding effect on slag. Yang et al. [15]'s research on alcohol ether side chains showed that the molecular weight of the grinding aid has no significant impact on its grinding performance, and the key influencing factor is the side chain structure in the molecule.

Research on polymer-based grinding aids, particularly regarding how the side chain structures of polymer molecules affect the grinding and hydration processes of slag, remains relatively scarce. Studies [16–18] have shown that polycarboxylate polymers have a strong binding affinity for Ca^{2+}, which can interfere with the nucleation of C-S-H gel; the formation of C-S-H gel only proceeds smoothly when Ca^{2+} is supersaturated. Research by [19] found that polycarboxylate ether (PCE) forms complexes with Ca^{2+} in the liquid phase of hydrating cement, thereby inhibiting the dissolution of C_3A and the growth of ettringite (AFt). Previous research [20] demonstrated that the sulfonic acid groups ($-SO_3^-$) in sulfonated poly (2-acrylamido-2-methylpropanesulfonic acid) (PAMPS) can not form complexes with Ca^{2+}. However, they can enrich Ca^{2+} at the interface through electrostatic attraction, thereby promoting the formation of C–S–H nanocrystals.

In summary, research on amine- and polymer-based grinding aids, especially regarding how polymer molecular structures regulate grinding efficiency and the hydration process, remains relatively limited. Based on this, in this study, low-molecular-weight polymers were synthesized with 2-acrylamido-2-methylpropanesulfonic acid (AMPS), hydroxypropyl acrylate (HPA) and diethylene glycol monovinyl ether (DEGVE) as monomers, sodium hypophosphite (SHP) as chain transfer agent and ammonium persulfate (APS) as initiator. Subsequently, the obtained polymers were compounded with polyhydric alcohols to prepare polymer grinding aids applicable to ground blast furnace slag (GBFS). AMPS was introduced as a functional monomer to incorporate highly polar sulfonic acid groups into the polymer structure. By adjusting the AMPS dosage, the overall structure of the polymer could be regulated, including the relative proportion of sulfonic acid groups and hydrophobic segments, as well as the molecular flexibility of the copolymer. These structural changes may jointly affect the adsorption behavior and dispersion performance of the polymer toward cement and GBFS particles [21–23]. It should be noted that variations in AMPS dosage may simultaneously influence multiple structural factors of the polymer, including sulfonic group density, molecular flexibility, and molecular weight distribution. Therefore, the observed performance differences are likely associated with coupled structural effects rather than a single parameter alone. In this study, the discussion is mainly focused on the overall influence of AMPS-regulated polymer structure on grinding and hydration behavior.

2 Materials and experimental methods

2.1 Materials

AMPS, HPA, DEGVE, sodium hypophosphite, ammonium persulfate (APS), and polyhydric alcohol were all of analytical purity and obtained from Shanghai Aladdin Biochemical Technology Co., Ltd. Granulated blast furnace slag (GBFS) was supplied by Huaxin Cement Co., Ltd., its chemical composition is shown in Table 1. An alkanolamine-based grinding aid HE-5 produced by Luoyang Hong'en New Building Materials Co., Ltd. was selected as the reference sample. P·I 42.5 cement from Huaxin Cement Co., Ltd. was used to prepare blended cement paste samples for hydration properties evaluation and mortar samples for activity evaluation of GBFS.

2.2 Methods

Grinding tests were carried out using a φ500 mm × 500 mm horizontal batch ball mill and the motor power is 1.5 kW. A multi-size steel ball system (10–40 mm) was employed as the grinding media to enhance the synergistic effects of impact and abrasion. The steel ball loading rate and material loading rate were 35% and 12%, respectively, and the mill speed was set at 48 r/min. The grinding duration was 80 min, and dry grinding was adopted. All experiments were conducted at (25 ± 2)°C. The grinding aid was added dropwise to the slag at a dosage of 0.05% by mass, followed by grinding for 80 min to obtain slag powder samples for subsequent analysis.

Referring to the national standard GB/T 26748-2011 "Cement Grinding Aids", the specific surface area of the sample was determined using an FBT9 Blaine automatic specific surface area analyzer, and the average value of three parallel experimental results was taken as the final specific

Table 1 Chemical composition of GBFS

	SiO_2	Al_2O_3	Fe_2O_3	CaO	MgO	$K_2O + Na_2O$	SO_3	TiO_2	Loss
GBFS	35.14	13.62	0.77	39.42	7.25	1.37	0.58	0.32	1.53

surface area of the sample. The 45 µm sieve residue of GBFS was determined using an FSY150 cement fineness negative pressure sieve analyzer (the calculation method is shown in Formula (1)), and the average value of three parallel experimental results was also taken as the final sieve residue.

$$\textit{Sieve}\ \text{residue}(\%) = \frac{\text{Quality of the remaining sample}}{\text{The initial mass of the sample}} \times 100\% \quad (1)$$

Particle size distribution determination: The particle size distribution of GBFS particles was measured using a Mastersizer 3000 laser particle size analyzer, with ethanol as the dispersion medium. Ultrasonic treatment was applied to ensure uniform dispersion of particles.

Polymer molecular weight distribution determination: The molecular weight distribution of the polymer was determined using a Waters 1515 gel permeation chromatograph. After detection, parameters such as number-average molecular weight (Mn), weight-average molecular weight (Mw), Z-average molecular weight (Mz), molecular weight distribution index, and polydispersity index of the polymer were calculated.

Fourier transform infrared (FT-IR) spectroscopy analysis: The infrared absorption spectrum of the polymer was scanned using a Fourier transform infrared spectrometer (AutosystemXL/I-series/Spectrum 2000) with a scanning range of 400 cm^{-1} ~4000 cm^{-1} and a resolution of 4 cm^{-1}.

X-ray diffraction (XRD) analysis: The phase development was investigated using an Empyrean X-ray diffractometer (Panaco B.V., the Netherlands) equipped with a CuKα radiation source and a 0.5° fixed divergence slit. The X-ray tube was operated at 45 kV and 40 mA, and data were collected in a continuous scanning mode from 5° to 50°.

Scanning electron microscopy (SEM) analysis: The microstructure of hydrated samples at different curing ages was characterized using a JSM6390 scanning electron microscope. Before testing, the samples were sputter-coated with gold to observe their surface morphological characteristics.

GBFS activity determination: In accordance with the national standard GB/T 12957-2005 "Test Methods for Activity of Industrial Waste Residues Used as Cement Admixtures", 30% GBFS was mixed into cement. The activity of GBFS was determined by comparing the 28 d compressive strength of the mixed system with that of the pure cement sample.

Setting time and normal consistency determination: In accordance with the national standard GB/T 1346-2011, a Vicat apparatus was used to determine the setting time and the water requirement for normal consistency. The paste where the test rod sinks into the paste and is 6 mm ± 1 mm away from the base plate is regarded as the normal consistency paste. When the test needle sinks to 4 mm ± 1 mm away from the base plate, it is judged as the initial setting state; when the test needle sinks into the test specimen by 0.5 mm, it is judged as the final setting state.

3 Results and discussion

3.1 Preparation of polymer grinding aid

The chain transfer agent SHP and HPA with various molar ratios were mixed in an aqueous solution with a total mass fraction of 50% and placed in a four-necked flask. A certain amount of AMPS and DEGVE was mixed in an aqueous solution with a total mass fraction of 30%, denoted as Solution A. APS was weighed and prepared into an aqueous solution with a mass fraction of 5%, denoted as Solution B. Nitrogen gas was introduced into the four-necked flask, and the mixture was heated to 50°C under constant stirring. Subsequently, Solution A and Solution B were added dropwise at a constant rate within 1.5 h and the reaction was maintained for another 2 h at 50°C. Then, the mixture was neutralized to pH of 7 ± 0.2 with an appropriate amount of 8 mol/L NaOH solution to obtain the polymer component (see Figure 1). Finally, the polymer grinding aid was prepared by mixing the synthesized polymer with polyhydric alcohols at a mass ratio of 1:4.

During the preparation process, the strongly electron-withdrawing sulfonic acid groups in AMPS could adjust the electron density of double bonds and facilitate free radical polymerization. Hydroxyl groups are introduced into the molecular structure by HPA and sodium hypophosphite, while diether bonds are introduced by DEGVE. The sulfonic acid groups introduced by AMPS can promote the local enrichment of Ca^{2+} via electrostatic

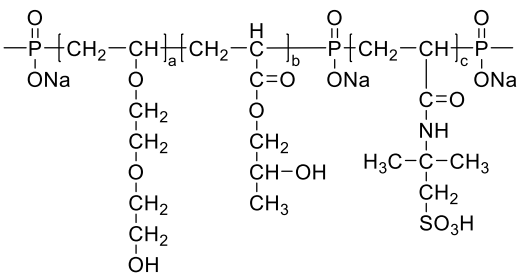

Figure 1 The molecular structure of polymer fabricated in this work

interactions [20], The hydroxyl groups introduced by HPA and sodium hypophosphite can act as hydrogen bond donors or acceptors, thereby contributing to possible hydrogen bond-related interactions with cement particles. As a comonomer, DEGVE contains two ether bonds in its molecular structure [24]. This not only enhances the mobility of the polymer chains, but also generates steric hindrance, thereby improving the dispersion performance of the system [22].

Based on the above molecular structure design concept, the molar ratio of DEGVE to AMPS was set within the range of 1:2.55 to 1:3.00, and the molar ratio of HPA was fixed at 0.5 in the experiment. Polymer samples I, II and III were screened via preliminary tests, and their molar ratios of DEGVE:AMPS:HPA were 1:2.55:0.5, 1:2.65:0.5 and 1:2.75:0.5, respectively.

Comparative analysis of experimental data from multiple groups with different APS dosages and chain transfer agent dosages showed that when the APS dosage was 1.28% of the total monomer mass and the chain transfer agent dosage was 5.14% of the total monomer mass, the GBFS particles treated with the prepared polymer grinding aid had smaller fineness and higher specific surface area. Meanwhile, the hydroxyl content in the polymer main chain was appropriate, which could effectively stabilize the material layer and promote the transfer of mechanical force from the grinding medium between materials.

3.2 Structure characterization and performance evaluation of polymer

The infrared spectrum of the polymeric component of the grinding aid is presented in Figure 2. A hydroxyl stretching vibration peak was observed at 3447 cm^{-1}. Stretching vibration peaks of methyl and methylene groups appeared at 2807 cm^{-1}. A stretching vibration peak corresponding to the carbonyl group in ester moieties was detected at 1724 cm^{-1}. The characteristic absorption peak of the amide carbonyl and the bending vibration peak of the amino group were found at 1633 cm^{-1} and 1499 cm^{-1}, respectively. A stretching vibration peak of the S=O double bond in sulfonic acid

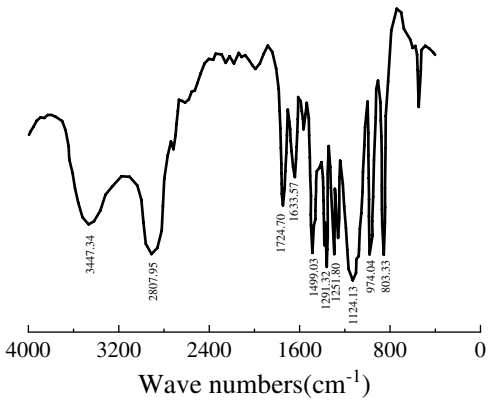

Figure 2 FTIR curve of fabricated grinding aid polymer

groups was observed at 1291 cm^{-1}, and a P=O stretching vibration peak at 1251 cm^{-1}. In addition, an ether bond stretching vibration peak was identified at 1124 cm^{-1}. These results confirm that the as-prepared polymer satisfies the structural design requirements.

3.3 Effect of AMPS-regulated polymer structure on grinding performance

Figure 3 shows the effects of the AMPS molar ratio of polymer on the grinding performance of polymer grinding aid and the polymer molecular weight. The specific data of GBFS particle size distribution under different conditions are shown in Table 2. In the molecular structure of the polymer grinding aid, AMPS served as a functional component that provides highly polar sulfonic acid groups [22]. By adjusting the AMPS content, the overall structure of the polymer could be regulated, including the relative proportion of polar sulfonic acid groups and hydrophobic segments, which may further affect the adsorption behavior and dispersion performance of the copolymer toward cement and GBFS particles [23]. Thus, as shown in the figure, at a low AMPS molar ratio, the amount of anchoring groups, such as sulfonic acid groups, was insufficient. This may limit the electrostatic attraction between the polymer and

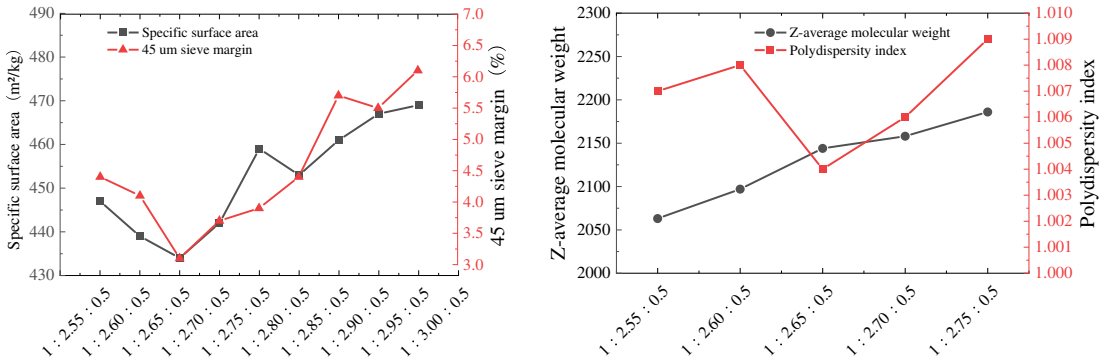

(**a**) Molar ratio of DEGVE: AMPS:HPA (**b**) Molar ratio of DEGVE: AMPS:HPA

Figure 3 The influence of DEGVE: AMPS:HPA molar ratio on grinding efficiency (a) and molecular weight (b)

Table 2 AMPS molar ratio and particle size distribution (All results are presented as mean ± standard deviation based on three parallel tests)

Sample	Molar Ratio of DEGVE: AMPS:HPA	Particle Size Distribution (%)					D50 (μm)	Specific Surface Area (m^2/kg)	Sieve Residue (%)
		0~3 μm	3~32 μm	32~64 μm	64~80 μm	>80 μm			
Blank (a)	–	17.09	42.21	27.60	8.21	4.89	16.02 ± 0.20	372 ± 4	9.8 ± 0.25
Alkanolamine-based grinding aid (b)	–	23.59	48.98	20.51	5.08	1.84	9.32 ± 0.14	440 ± 5	2.3 ± 0.27
Polymer grinding aid I (c)	1:2.55:0.5	20.87	51.81	23.81	2.59	0.92	10.97 ± 0.13	431 ± 5	4.7 ± 0.15
Polymer grinding aid II (d)	1:2.65:0.5	22.31	53.03	23.02	1.13	0.51	9.81 ± 0.12	434 ± 6	3.1 ± 0.2
Polymer grinding aid III (e)	1:2.75:0.5	19.02	50.13	26.62	3.21	1.02	12.45 ± 0.17	449 ± 8	4.2 ± 0.25

Ca^{2+} on the GBFS particle surface [22–24], resulting in weakened adsorption of polymer on the GBFS particle surface and poor dispersion of GBFS particles [11, 25, 26]. Consequently, it resulted in a relatively high proportion of coarse particles (>32 μm). When the molar ratio of AMPS reached 2.65, the increase in sulfonic acid groups may enhance the adsorption of the polymer on the particle surface, which was likely achieved through stronger electrostatic attraction between the sulfonic acid groups and Ca^{2+}, thereby improving the dispersion performance of GBFS particles. This balanced adsorption–dispersion behavior effectively reduced particle agglomeration. As a result, the proportion of coarse particles (>80 μm) decreased to 0.51%, and the D50 value decreased to 9.81 μm.

However, when the AMPS content was further increased, the structural changes in the polymer may lead to excessively strong electrostatic attraction between the sulfonic acid groups and Ca^{2+}. The resulting excessive dispersion effect may disrupt hydrogen bond-related intermolecular interactions and the stability of the adsorption layer. These interactions are considered beneficial for the formation of a stable material layer during the grinding process, thereby leading to particle size rebound [27, 28] (D50 increased to 12.45 μm) and a deterioration in particle size distribution [22, 23].

The effect of different grinding aids on the surface morphology of GBFS particles was observed by SEM as shown in Figure 4. The surface of GBFS particles in the blank group (Figure 4a) is relatively smooth; the surface of GBFS particles mixed with alkanolamine reference sample (Figure 4b) has cracks, but there are still smooth areas locally.

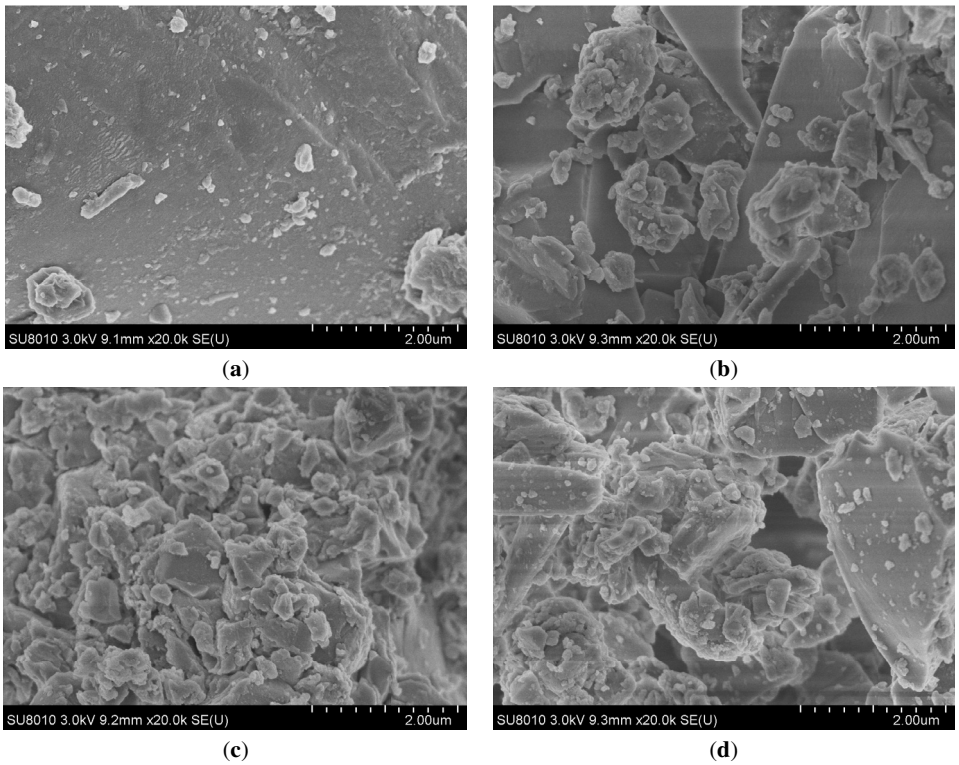

Figure 4 The SEM of GBFS after grinding. Blank slag sample (a), slag sample treated with alcoholamine grinding aid (b), slag sample treated with polymer grinding aid II (c), and slag sample treated with polymer grinding aid III (d)

This indicates that although the alkanolamine grinding aid showed a certain effect in stabilizing the material layer, it was difficult to effectively disintegrate coarse GBFS particles larger than 64 µm because of the insufficient amount of dispersion groups and low molecular weight (detailed data are shown in Table 2) [29]. The surface of the GBFS particles mixed with polymer grinding aid II (Figure 4c) became rougher, and Table 2 shows that the proportion of coarse particles larger than 64 µm decreased significantly. For the GBFS particles treated with polymer grinding aid III (Figure 4d), the rough particle surface of GBFS may be attributed to the relatively high methyl group content in its molecular structure [22, 23]. The content of coarse GBFS particles larger than 64 µm, particle fineness, and specific surface area showed a rebound compared with those of the GBFS particles mixed with polymer grinding aid II (Figure 4c) (detailed data are shown in Table 2).

3.4 Effect of AMPS-regulated polymer structure on hydration behavior

Table 3 shows the results of setting properties and workability of cement paste blended with GBFS treated by different grinding aids. In the case of polymer grinding aid, the water demand for standard consistency gradually increased with the increased AMPS dosage in polymer grinding aid. This may be attributed to the increased proportion of hydrophobic chain segments [23], which further enhanced the dispersion performance of the grinding aid and may have promoted the participation of more GBFS glass phases in the hydration reaction. On the one hand, this leads to an increase in the water requirement for normal consistency, so that the number of cementitious materials that can participate in early hydration in the paste increases accordingly [30]. This further reduces the hydration heat and slightly inhibits the hydration process, ultimately resulting in prolonged initial and final setting times [30]. On the other hand, the vitreous particles in GBFS can fill the gaps between cement particles and play a lubricating role, increasing the fluidity of the mortar [31]. In addition, the water requirement for normal consistency of the reference sample mixed with alkanolamine-based grinding aid is slightly higher than that of the blank control group. The reason is that the dispersion capacity of alkanolamine-based grinding aids is weak, which cannot effectively promote the dense vitreous phase in GBFS to participate in the early hydration reaction [7, 8, 32].

By adjusting different molar ratios of AMPS, grinding aids with varying polymer structures were prepared. The compressive strength of mortar incorporating grounded GBFS with different grinding aids are shown in Table 4. The 7 d and 28 d compressive strengths of the blank sample (a) were 35.4 MPa and 49.3 MPa, respectively. The 7 d and 28 d compressive strengths of the sample containing the alkanolamine grinding aid (b) were 34.7 MPa and 50.8 MPa, respectively. The sample containing polymer grinding aid I (c) showed the highest 28 d compressive strength among all the samples considered. According to the above results, the polymer grinding aids prepared with an appropriate AMPS dosage were beneficial for the coordinated development of compressive strength. However, when the AMPS dosage was excessively high (Polymer grinding aid III), although the early-age strength development was promoted, it showed a certain adverse effect on the late-age strength growth. In the case of samples containing polymer grinding aids, the sample containing polymer grinding aid II (d) exhibited the lowest D50 value and the most balanced particle size distribution and sieve residue. In contrast, although the alkanolamine grinding aid showed slight advantages in grinding efficiency indicators such as specific surface area and sieve residue of GBFS, the polymer grinding aid systems exhibited overall superior mechanical properties.

In this study, the polymer grinding aid not only played the basic roles of physical dispersion and grinding assistance, but also exhibited a certain improvement effect on the compressive strength of GBFS, thereby simultaneously influencing particle refinement behavior and impacting hydration

Table 3 **Test results of paste performance (All results are presented as mean ± standard deviation based on three parallel tests)**

Sample	Molar Ratio of DEGVE: AMPS:HPA	Specific Surface Area (m^2/kg)	Sieve Residue (%)	Water Requirement/%	Setting Time/min		Fluidity of Cement Mortars/mm
					Initial Setting	Final Setting	
Blank (a)	–	372 ± 4	9.8 ± 0.25	26.60 ± 0.15	146 ± 3	208 ± 4	175 ± 3
Alkanolamine-based grinding aid (b)	–	440 ± 5	2.3 ± 0.27	26.85 ± 0.12	156 ± 3	209 ± 4	182 ± 3
Polymer grinding aid I (c)	1:2.55:0.5	431 ± 5	4.7 ± 0.15	27.00 ± 0.15	152 ± 2	212 ± 3	187 ± 4
Polymer grinding aid II (d)	1:2.65:0.5	434 ± 6	3.1 ± 0.2	27.20 ± 0.15	155 ± 2	216 ± 3	189 ± 3
Polymer grinding aid III (e)	1:2.75:0.5	449 ± 8	4.2 ± 0.25	27.20 ± 0.18	149 ± 3	231 ± 5	201 ± 4

Table 4 Test results of mortars strength (All strength results are expressed as mean ± standard deviation based on three parallel tests)

Sample	Molar Ratio of DEGVE: AMPS:HPA	Dosage of Initiator (%)	Chain Transfer Agent (%)	Compressive Strength (MPa)			28 d Activity Index (%)
				3 d	7 d	28 d	
Blank (a)	–	–	–	16.4 ± 0.4	35.4 ± 0.6	49.3 ± 0.8	94 ± 1.8
Alkanolamine-based grinding aid (b)	–	–	–	17.1 ± 0.3	34.7 ± 0.5	50.8 ± 0.7	97 ± 1.5
Polymer grinding aid I (c)	1:2.55:0.50	1.28	5.14	17.6 ± 0.4	37.0 ± 0.6	54.0 ± 0.9	103 ± 2.1
Polymer grinding aid II (d)	1:2.65:0.50	1.28	5.14	18.8 ± 0.3	37.6 ± 0.5	53.0 ± 0.8	101 ± 1.7
Polymer grinding aid III (e)	1:2.75:0.50	1.28	5.14	18.3 ± 0.4	38.2 ± 0.6	51.3 ± 0.7	98 ± 1.9

kinetics. Therefore, the optimal formulation was determined through the comprehensive consideration of grinding efficiency indicators and mechanical properties, rather than based only on a single parameter, such as D50 or 28 d mechanical strength. When evaluating the blank sample, the sample containing the alkanolamine grinding aid, and the sample containing polymer grinding aids, the mechanical properties of the polymer grinding aid systems were superior to those of the blank sample and the alkanolamine grinding aid sample. In addition, among the samples containing polymer grinding aids, the sample containing polymer grinding aid II (d) exhibited the optimal grinding efficiency indicators, including D50 and particle fineness. Therefore, based on the comprehensive evaluation of grinding performance and mechanical properties, polymer grinding aid II could be regarded as the most well-balanced formulation in the polymer system.

3.5 Hydration property

3.5.1 Evolution of hydration heat

Hydration heat test results are presented in Figure 5. The main exothermic peak of the blank sample (a) appears at approximately 12 h. The addition of both polymer grinding aids (c,d,e) and alkanolamine grinding aids (b) delays the occurrence of the second exothermic peak. This may be related to the hydroxyl groups present in both types of grinding aids, which could interact with particle surfaces through hydrogen-bond-related interactions and thereby retard the hydration process [8]. Owing to the higher hydroxyl density in alkanolamine grinding aids, their retarding effect on the hydration exothermic peak is more significant [8]. With the increase in AMPS dosage, the polymer structure underwent gradual changes, in which the proportions of sulfonate groups and hydrophobic segments gradually increased. This may have enhanced the adsorption and anchoring performance, improved the dispersion of the cement paste to a certain extent, and accelerated the early hydration process, thereby resulting in higher heat release than that of the sample with alkanolamine. The cumulative heat release results showed that both the polymer (c,d,e) and alkanolamine grinding aids (b) could increase the cumulative heat release of cement within 3 d [7, 32, 33].

Nevertheless, cement samples incorporating polymer grinding aids (c,d,e) display higher cumulative heat release than those with alkanolamine grinding aids (b). This may be attributed to the dispersion characteristics of the alcohol–ether

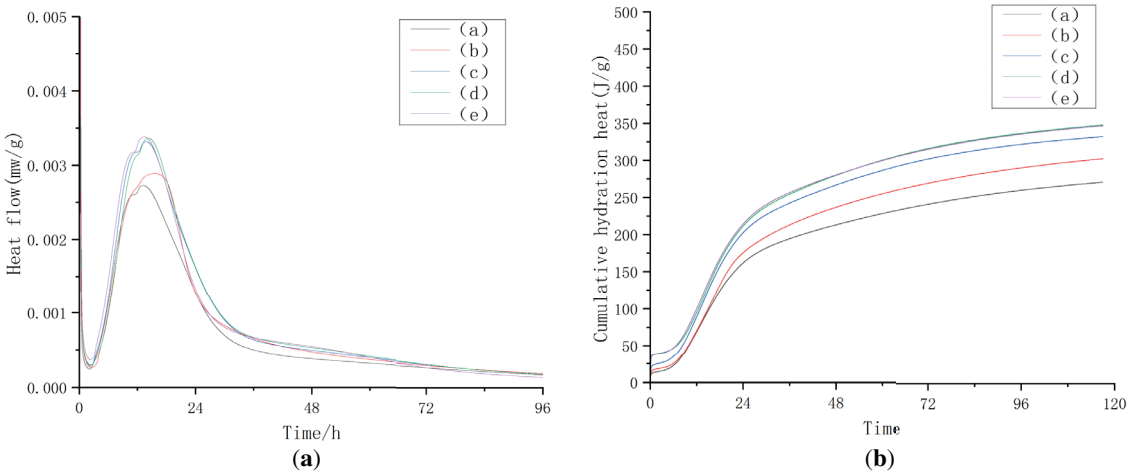

Figure 5 Hydration heat flow (a) and cumulative hydration heat (b)

side chains and hydrophobic segments in the polymer, which may affect hydroxyl-related intermolecular interactions, thereby weakening the retarding effect on the cement hydration process [22, 24, 32].

3.5.2 Micro-morphology of hydration products

SEM images of the hydration products for different samples at curing ages of 7 d and 28 d are presented in Figures 6 and 7, respectively. The hydration products of blank sample (a) showed a

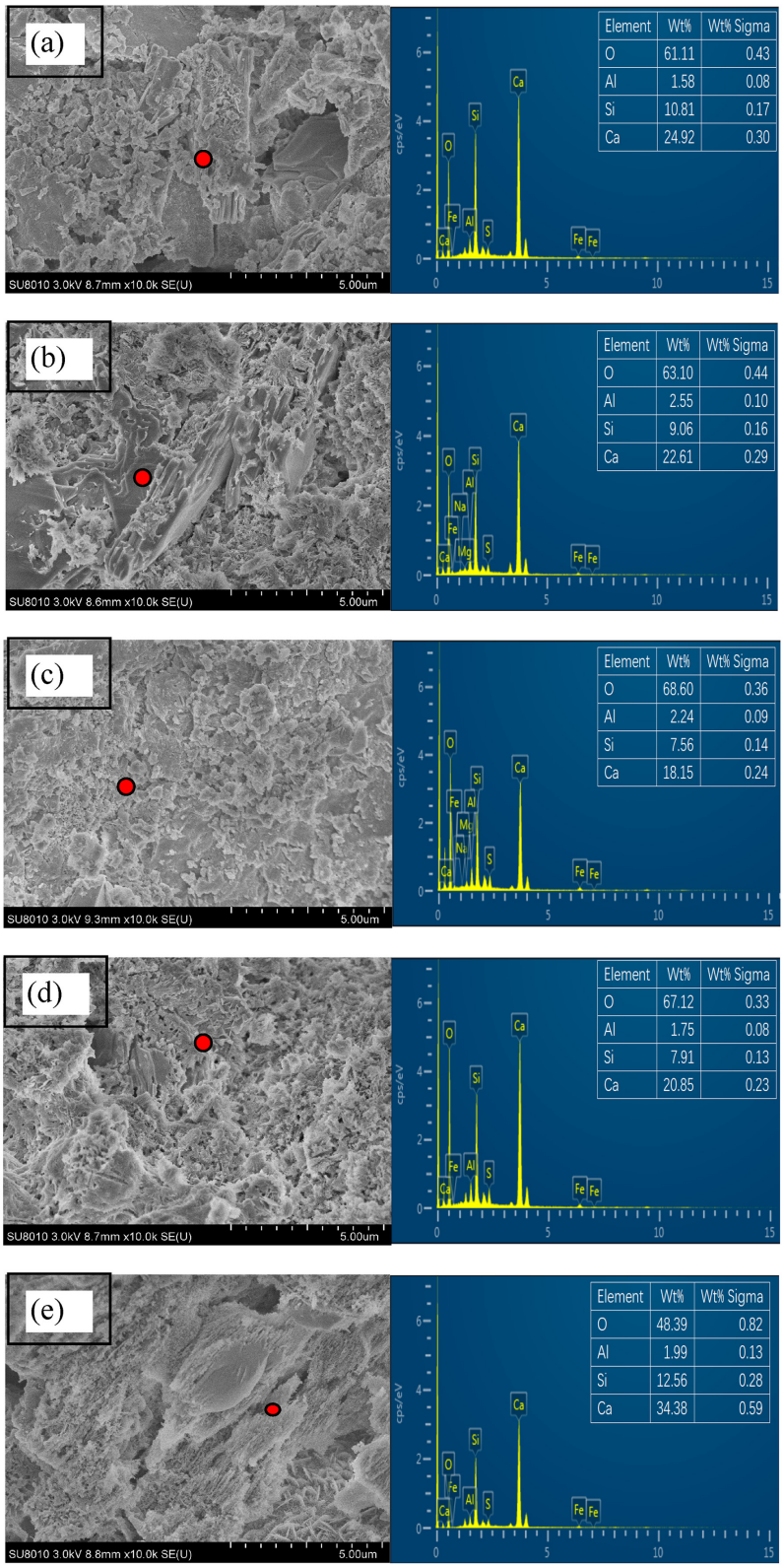

Figure 6 SEM and EDS images of pastes after 7 d of hydration. Blank sample (a), sample mixed with alkanolamine grinding aid (b), sample mixed with polymer grinding aid I (c), sample mixed with polymer grinding aid II (d), sample mixed with polymer grinding aid III (e)

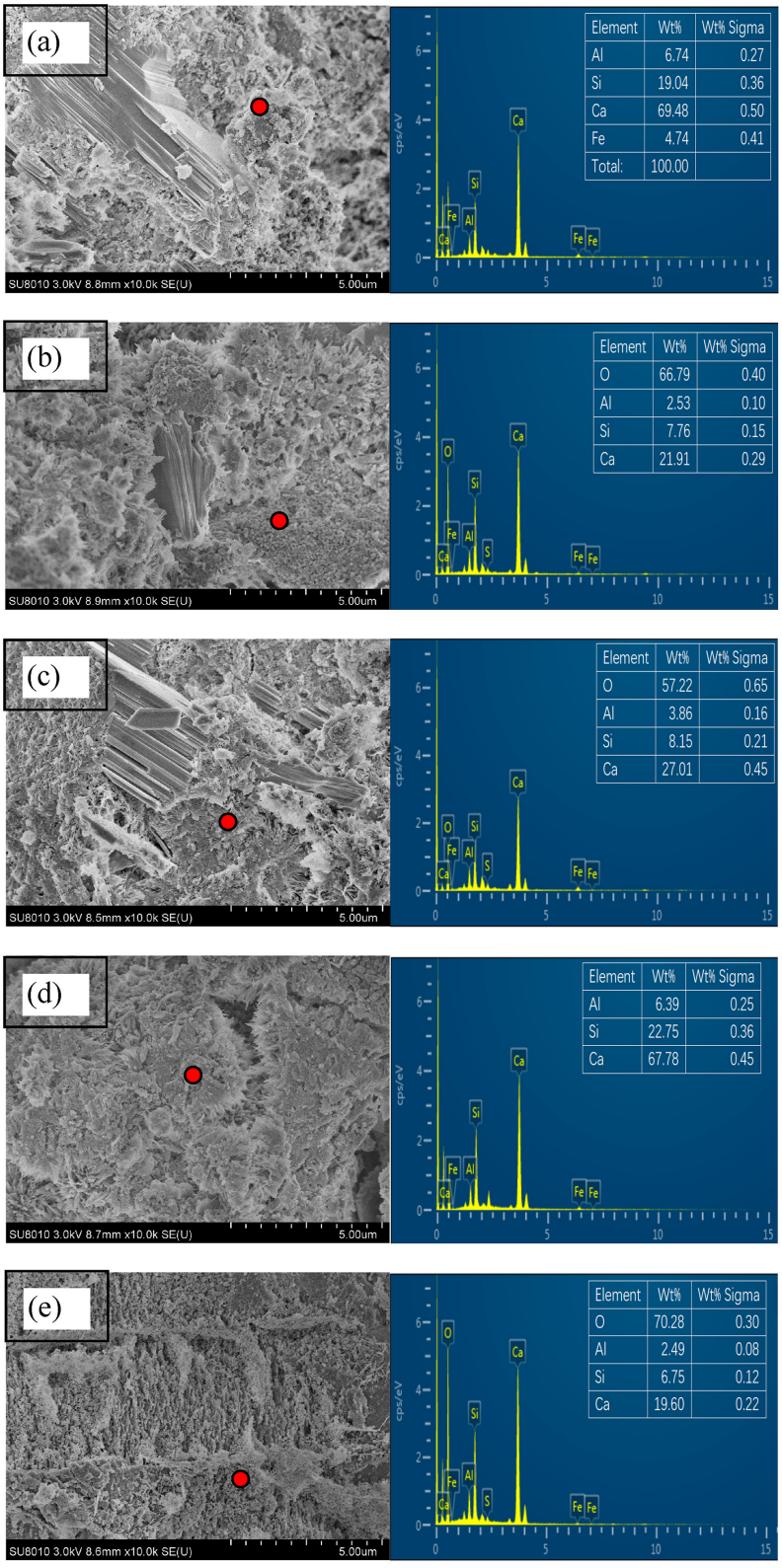

Figure 7 SEM and EDS images of pastes after 28 d of hydration. Blank sample (a), sample mixed with alkanolamine grinding aid (b), sample mixed with polymer grinding aid I (c), sample mixed with polymer grinding aid II (d), sample mixed with polymer grinding aid III (e)

smooth surface with obvious pores at age of 7 d (Figure 6a), and the Ca/Si ratio was 1.61, indicating the possible formation of low-density C–S–H with a relatively low degree of polymerization, which is consistent with the porous microstructure observed at this age. At 28 d (Figure 7a), the Ca/Si ratio increased to 1.75, suggesting that the hydration process may have been inhibited, resulting in relatively low strengths at both 7 d and 28 d. Compared with the blank sample (a), the sample

containing the alkanolamine grinding aid (b) showed slightly higher Ca/Si ratios at both curing ages, reaching 1.68 at 7 d and 1.85 at 28 d. This may be attributed to the presence of a certain amount of dispersing groups, which enhanced hydration activity and increased the formation of hydration products, thereby resulting in slight increases in both 7 d and 28 d strengths. The sample containing polymer grinding aid I (c) contained a relatively high proportion of hydrophobic side chains, which may enhance its dispersion performance and hydration reactivity. At 7 d, this treatment may have promoted the hydration of C_3S, and the Ca/Si ratio reached 1.92, and the 7 d strength was significantly higher than that of the blank sample (a). At 28 d, the Ca/Si ratio increased to 2.60, indicating that the hydration of C_3S may have been further promoted, leading to the formation of a relatively well-developed cross-linked network and a significant improvement in strength compared with the blank sample. The sample containing polymer grinding aid II (d) exhibited a Ca/Si ratio of 1.98 at 7 d, indicating further enhanced dispersion performance. In the hydration products, AFt and AFm appeared alternately and interwove with C–S–H gels. This was consistent with the Ca/Si ratio (1.98), suggesting that relatively well-developed C–S–H gel may have formed, which combined with AFt/AFm phases, thereby promoted a further increase in strength. At 28 d, the Ca/Si ratio was 2.32. Exposed AFt and AFm crystals and increased porosity were observed, which may be unfavorable for strength development. The sample containing polymer grinding aid III (e) exhibited a Ca/Si ratio of 2.10 at 7 d. At this stage, exposed AFt and AFm phases were observed, which were unfavorable for strength development. Nevertheless, the strong dispersion effect may have promoted the participation of more glassy phases in slag hydration and favored the formation of C–S–H, and therefore the strength still increased. At 28 d, the Ca/Si ratio decreased to 2.03. This may have accelerated the dissolution of Al^{3+} [34–36], resulting in the formation of loosely structured C–S–H with a relatively low degree of polymerization, as reflected by the variation in the Ca/Si ratio. This was also consistent with the observed porous and less compact microstructure, thereby leading to a significant reduction in strength.

3.5.3 XRD analysis of hydration products

Figure 8 shows the XRD patterns of different samples cured for 7 d and 28 d. The characteristic peaks of each mineral phase in the spectrum can be clearly observed.

The 7 d XRD patterns show that the blank sample (a) still exhibited relatively obvious C_3S characteristic peaks, indicating that a certain amount of unreacted clinker minerals remained in the system. In contrast, the sample containing the alkanolamine grinding aid (b) [33] showed a slight decrease in the C_3S peak intensity and an increase in the CH peak intensity, indicating that it may promote the hydration of silicate minerals to a certain extent. Compared with the sample containing the alkanolamine grinding aid (b), the samples containing polymer grinding aids (c–e) exhibited more obvious phase composition changes at 7 d. In some samples, the AFt peak intensity further increased, while AFm peaks also appeared, indicating that the amount of aluminate hydration products may increase and the aluminate phase reaction became relatively more active [3]. Meanwhile, some polymer samples exhibited slightly higher CH peak intensities than the alkanolamine sample, suggesting that the hydration of silicate minerals may have been relatively more sufficient.

At 28 d, a certain C_3S peak could still be observed in the blank sample (a), indicating that some minerals remained insufficiently reacted during the later hydration stage. In the sample containing the alkanolamine grinding aid (b), the

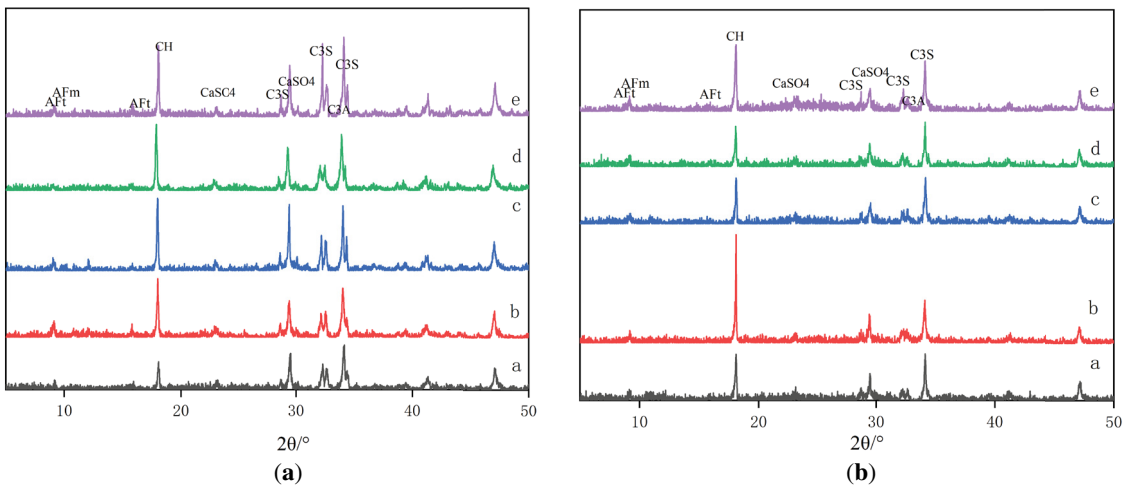

Figure 8 XRD Analysis of pastes with the different grinding aids (a) 7 d and (b) 28 d

C_3S peak intensity decreased compared with that of the blank sample, indicating that the silicate hydration products were still evolving during the later stage. Compared with the sample containing alkanolamine grinding aid (b), the samples containing polymer grinding aids (c–e) exhibited relatively more obvious AFm peaks and slightly weakened AFt peaks at 28 d, indicating that part of the AFt may have further transformed into AFm. Meanwhile, some samples containing polymer grinding aids showed a further decrease in the C_3S peak intensity, indicating that the continued hydration phenomenon during the later stage was relatively more pronounced.

Overall, the XRD results showed good consistency with the SEM observations and the strength development trends obtained from the mechanical property tests, and these results can serve as supporting evidence for the influence on hydration performance.

It should be noted that although comprehensive quantitative phase analysis was not performed, the relative variation of characteristic peak intensities can provide semi-quantitative information on phase evolution. Combined with SEM microscopic observations and mechanical property results, these data can serve as auxiliary supporting evidence.

3.5.4 Infrared spectra of hydration products

The infrared spectra of hydration products of different samples at 7 d and 28 d curing ages are shown in Figures 9 and 10. The detailed analysis is as follows: the blank control group (a) shows insufficient dispersion capacity at both 7 d and 28 d curing ages, with low transmittance at

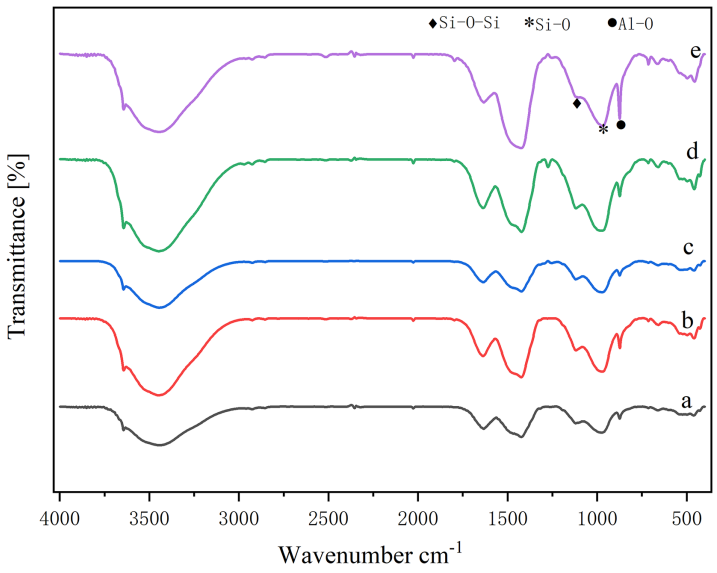

Figure 9 FTIR analysis of pastes after 7 d of hydration

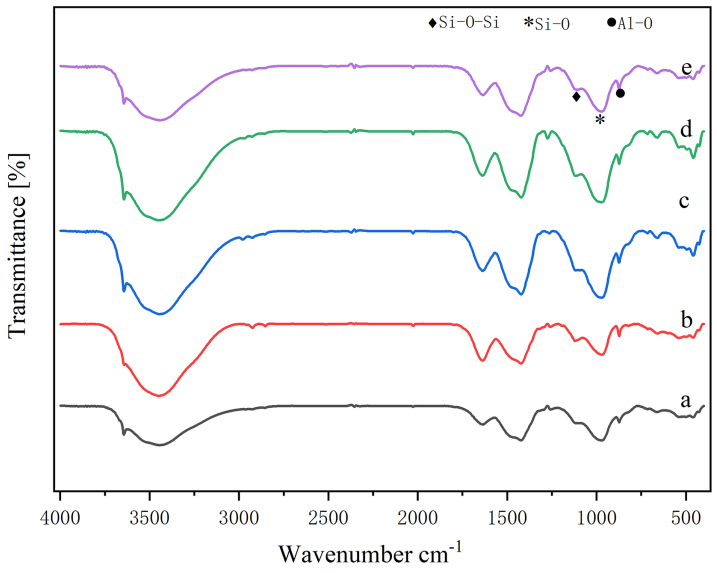

Figure 10 FTIR analysis of pastes after 28 d of hydration

wave numbers of 1119.25 cm^{-1}, 983.79 cm^{-1}, and 873.64 cm^{-1} [37]. This indicates that the contents of Si-O-Si, Si-O, and Al-O functional groups in the sample are low, and the degree of hydration reaction is low [37]. For the alkanolamine-based grinding aid reference sample (b), the dispersion capacity is slightly improved at 7 d curing age, but hydroxyl groups hinder the dissolution of Al^{3+} [38]. Only a small amount of Al^{3+} dissolves until 28 d curing age, thereby forming dense C-A-S-H gel [38]. The polymer grinding aid I (c) has significantly improved dispersion capacity, showing high transmittance at wave numbers of 1119.25 cm^{-1}, 983.79 cm^{-1}, and 873.64 cm^{-1} at both 7 d and 28 d curing ages [37]. This indicates that the contents of Si-O-Si, Si-O, and Al-O functional groups in the sample are high. The polymer grinding aid II (d) can promote the dissolution of Al^{3+} at both 7 d and 28 d curing ages, and the dissolved Al^{3+} can combine with siloxane precursors [39, 40]. The polymer grinding aid III (e) has the problem of excessive dispersion. At 7 d curing age, it shows high transmittance at 873.64 cm^{-1}, indicating a high content of Al-O functional groups, i.e., excessive dissolution of Al^{3+}, which leads to disordered distribution of aluminum-containing products and enrichment of Al^{3+} on the particle surface. At 28 d curing age, the excessively dissolved Al^{3+} will inhibit the polymerization of C-S-H gel, hinder the cross-linking of siloxane precursors [41].

4 Conclusions

In this study, the polymer structure was regulated by adjusting the AMPS dosage, thereby influencing multiple structural characteristics of the polymer system. The effects of molecular structure on the grinding and hydration properties of GBFS were systematically investigated. The main conclusions are as follows:

(1) During the grinding process, the polymer grinding aids acted on the surface of GBFS particles and promoted particle breakage. The selected polymer grinding aid provides a better balance between particle-size distribution and strength development, while some individual fineness parameters remain comparable to or slightly less favorable than the alkanolamine reference. Polymer grinding aid II possessed an appropriate molecular structure, which effectively reduced the content of coarse GBFS particles larger than 64 µm, moderately increased the specific surface area, and made the particle surface rougher. In contrast, the higher AMPS dosage in polymer grinding aid III led to an excessively large specific surface area and a decrease in the 28 d mechanical properties.
(2) Adjustment of AMPS dosage alters the molecular structure of polymers, thereby endowing the polymer grinding aids with he effects of physical dispersion and compressive strength improvement. Owing to the molecular structure formed by an appropriate AMPS dosage, polymer grinding aid II could provide an effective dispersion effect, promote the participation of more glassy phases in the hydration reaction, increase the water absorption and fluidity, and prolong the setting time, thereby significantly improving the 3 d compressive strength.
(3) Microstructural analysis shows that, variations in molecular structure caused by different AMPS dosages affect the dissolution behavior of Al^{3+} and the subsequent interactions between Al^{3+} and silicate precursors. Reasonable adjustment of AMPS dosage endows polymer grinding aid II with optimal molecular structure, which promotes the formation of abundant C-A-S-H gels and develops dense and well-organized microstructure. In comparison, the excessive AMPS content in polymer grinding aid III changes the molecular structure unfavorably, hinders the formation of C-S-H gels and weakens interfacial interactions, consequently resulting in loose hydration microstructure.

Acknowledgement

Not applicable.

Funding Statement

The authors received no specific funding for this study.

Author Contributions

Conceptualization, Kai Ke; methodology, Kai Ke; software, Xiang Li; validation, Xiang Li; formal analysis, Kai Ke; investigation, Xiang Li; resources, Kai Ke; data curation, Xiang Li; writing—original draft preparation, Xiang Li; writing—review and editing, Kai Ke, Xiang Li and Yingbin Wang; visualization, Xiang Li; supervision, Kai Ke; project administration, Kai Ke. All authors reviewed and approved the final version of the manuscript.

Availability of Data and Materials

All data supporting the results of this study are included within the article.

Ethics Approval

Not applicable.

Conflicts of Interest

The authors declare no conflicts of interest.

REFERENCES

[1] Li C, Sun H, Li L. A review: the comparison between alkali-activated slag (Si+Ca) and metakaolin (Si+Al) cements. Cem Concr Res. 2010;40(9):1341–9. doi:10.1016/j.cemconres.2010.03.020.
[2] Jonczy I, Grzesik B, Wieczorek AN, Gerle A, Nuckowski P, Staszuk M. Characteristics of the phase and chemical composition of blast furnace slag in terms of the possibility of its economic use. Gospodarka Surowcami Miner Miner Resour Manag. 2022;38(4):153–72. doi:10.24425/gsm.2022.143625.
[3] Shi MG, Ke GJ, Zou PY, Song BX, Tang XL, Jin D. Research progress of hydration, mechanical and dry shrinkage properties of alkali-activated slag cement. Bull Chin Ceram Soc. 2022;41(1):162–91. (In Chinese).
[4] Jiang C, Xia L, Li S, Li X, Chen Y, Liu J. Impact of ground granulated blast furnace slag on calcium leaching of low-heat Portland cement paste. Materials. 2024;17(15):3857. doi:10.3390/ma17153857.
[5] Lee J, Lim A, Kang H, Jeon D, Lee N, Poon CS, et al. Understanding the effect of triethanolamine on grinding and hydration of blast furnace slag, focusing on the degrees of slag consumption and C(-A)-S-H formation. Constr Build Mater. 2025;458(12):139693. doi:10.1016/j.conbuildmat.2024.139693.
[6] Kim S, Yang J, Lee J, Poon CS, Moon J. Impact of triethanolamine on grinding and hydration performance of BOF steel slag blended cement. J Build Eng. 2025;101:111858. doi:10.1016/j.jobe.2025.111858.
[7] Hallet V, Hertel T, Eykens L, De Belie N, Pontikes Y. Alkanolamines as grinding aids and hydration enhancers in blended cements with iron-rich non-ferrous metallurgy slag. Constr Build Mater. 2025;470:140575. doi:10.1016/j.conbuildmat.2025.140575.
[8] He Y, Liu S, Zhang X, Liu W, Liao G, Xu M. Influence of triethanolamine on mechanical strength and hydration performance of blended cement containing fly ash, limestone and slag. J Build Eng. 2021;44:102879. doi:10.1016/j.jobe.2021.102879.
[9] Zhao Y, Shi Y, Wang L, Zhuang Y, Li Y, Chen G. Hydroxyl group-dependent effects of alkanolamine additives on rheology, hydration, and performance of early-strength cement slurries. Processes. 2025;13(9):2681. doi:10.3390/pr13092681.
[10] Chen J, Jia J, Zhu M, Zhang L. Advances of alkanolamine in hydration of Portland cement. Mater Today Commun. 2023;37(4):107129. doi:10.1016/j.mtcomm.2023.107129.
[11] Wang JF, Ma JK, Tang GB, Ma MX, Lan MZ, Cui SP. Preparation of glycerol phosphate and its effect on cement hydration. In: Proceedings of the 2018 China Cement Association Annual Conference on Cement Grinding Aids; 2018 Dec 27–29; Beijing, China.
[12] Yang S, Wang J, Cui S, Liu H, Wang X. Impact of four kinds of alkanolamines on hydration of steel slag-blended cementitious materials. Constr Build Mater. 2017;131(8–9):655–66. doi:10.1016/j.conbuildmat.2016.09.060.
[13] Xu M, Guo L, Wen J, Hu X, Wang L, Mo L. Mechanochemical activation of basic oxygen furnace slag: insights into particle modification, hydration behavior, and microstructural development. Materials. 2025;18(15):3687. doi:10.3390/ma18153687.
[14] Yang WL. Experimental study on several organic compounds and their homologues as slag grinding aids [master's thesis]. Luoyang, China: Henan University of Science and Technology; 2010.
[15] Yang HJ, Sun ZP, Plank J, Shui LL, Dong YW. Structure-activity relationship of polycarboxylate superplasticizers as grinding aids. J Build Mater. 2022;25(1):54–60. (In Chinese).
[16] Picker A, Nicoleau L, Nonat A, Labbez C, Cölfen H. Influence of polymers on the nucleation of calcium silicate hydrates. Cem Concr Res. 2023;174:107329. doi:10.1016/j.cemconres.2023.107329.
[17] Qiu H, Wu Y, Yu J, Wan Z, Zheng L, Chen H. Effect of calcium-silicate-hydrate (C-S-H) nano-crystals on the hydration rate and early strength of microwave-absorbing cement mortar containing magnetite (Fe_3O_4) powder. Ceram Int. 2023;49(23):39039–48. doi:10.1016/j.ceramint.2023.09.241.
[18] Baltakys K, Eisinas A, Doneliene J, Dambrauskas T, Sarapajevaite G. The impact of Al_2O_3 amount on the synthesis of CASH samples and their influence on the early stage hydration of calcium aluminate cement. Ceram Int. 2019;45(2):2881–6. doi:10.1016/j.ceramint.2018.07.286.
[19] Jansen D, Neubauer J, Goetz-Neunhoeffer F, Haerzschel R, Hergeth WD. Change in reaction kinetics of a Portland cement caused by a superplasticizer—calculation of heat flow curves from XRD data. Cem Concr Res. 2012;42(2):327–32. doi:10.1016/j.cemconres.2011.10.005.
[20] Zhang YR, Kong XM, Lu ZB, Lu ZC, Hou SS. Effects of the charge characteristics of polycarboxylate superplasticizers on the adsorption and the retardation in cement pastes. Cem Concr Res. 2015;67:184–96. doi:10.1016/j.cemconres.2014.10.004.
[21] Sekizkardes B, Su E, Okay O. Mechanically strong superabsorbent terpolymer hydrogels based on AMPS via hydrogen-bonding interactions. ACS Appl Polym Mater. 2023;5(3):2043–50. doi:10.1021/acsapm.2c02085.
[22] Duan H, Zhou T, Li B, Pang Y, Lou H, Yang D, et al. Synthesis, performance evaluation, and adsorption-dispersion mechanism of sulfonic acid-terminated long side chain polycarboxylate superplasticizers. Langmuir. 2024;40(47):24956–67. doi:10.1021/acs.langmuir.4c03026.
[23] Tian H, Zhang S, Liao J, Kong X, Wang Y. A novel type of superplasticizer with linear polymer structure for alkali-activated slag pastes. Constr Build Mater. 2025;494:143508. doi:10.1016/j.conbuildmat.2025.143508.
[24] Fan L, Xu F, Wang S, Yu Y, Zhang J, Guo J. A review on the modification mechanism of polymer on cement-based materials. J Mater Res Technol. 2023;26(6):5816–37. doi:10.1016/j.jmrt.2023.08.291.
[25] Wang JF. Structure-activity relationship and molecular structure design of cement grinding aids [dissertation]. Beijing, China: China University of Mining and Technology (Beijing); 2013.
[26] Rui Y, Huang T, Kong X, Zhao S, Li N, Zheng Y. The influence of *in-situ* polymerization of acrylamide on cement hydration. Mater Lett. 2026;402:139375. doi:10.1016/j.matlet.2025.139375.
[27] Weibel M, Mishra R. Comprehensive understanding of grinding aids. ZKG Int. 2014;6:28–39.
[28] Liu S, Zheng Y, Fan Q, Zhao J, Tan T. Mechanistic insights into the effect of triethanolamine on the grinding of cement-based monomineral materials: experiment and molecular dynamics. Colloids Surf A Physicochem Eng Aspects. 2026;742:140399. doi:10.1016/j.colsurfa.2026.140399.
[29] Przwara P, Kwade A. Grinding aids for dry fine grinding processes—part I: mechanism of action and lab-scale grinding. Powder Technol. 2020;375(1):146–60. doi:10.1016/j.powtec.2020.07.038.
[30] Shi Y Yang HM, Wang YC, Yang HQ, Li JZ. Effect of high-titanium slag on properties of cement-based composites. New Build Mater. 2009;36(9):1–4.
[31] Li M, Zhou P, Xiao W, Zhang C, Liu Z. Study on preparation and performance of fluid loss additive applied to chlorination titanium blast furnace slag. J Dispers Sci Technol. 2021;42(14):2163–72. doi:10.1080/01932691.2020.1808477.
[32] Kobya V, Kaya Y, Mardani-Aghabaglou A. Effect of amine and glycol-based grinding aids utilization rate on grinding efficiency and rheological properties of cementitious systems. J Build Eng. 2022;47(3–4):103917. doi:10.1016/j.jobe.2021.103917.
[33] Andrade Neto JS, Rodríguez ED, Monteiro PJM, De la Torre AG, Kirchheim AP. Hydration of C_3S and Al-doped C_3S in the presence of gypsum. Cem Concr Res. 2022;152:106686. doi:10.1016/j.cemconres.2021.106686.
[34] Shin JY, Hong JS, Suh JK, Lee YS. Effects of polycarboxylate-type superplasticizer on fluidity and hydration behavior of cement paste. Korean J Chem Eng. 2008;25(6):1553–61. doi:10.1007/s11814-008-0255-3.
[35] Guo A, Gao D, Sun Z, Feng H, Yu Z, Guo Z, et al. Hydration kinetics and mechanism of C_3S with cellulose nanocrystals. Cem Concr Compos. 2024;148(1):105447. doi:10.1016/j.cemconcomp.2024.105447.
[36] Li B, Wang L, Wang Z, Wang M. Influence of functional group's grafting position in polycarboxylate superplasticizer molecule on its dispersibility and mechanism. Cem Concr Res. 2025;195:107919. doi:10.1016/j.cemconres.2025.107919.
[37] Cui JM, Ma HR, Ma ZY, Ji LX, Wang S, Ba MF. Study on the effect and mechanism of secondary aluminum ash sintering slag grinding fine powder on the properties of modified magnesium sulfide cement-based materials. Mater Rep. 2025;39(15):154–62. (In Chinese). doi:10.1016/j.conbuildmat.2025.140428.
[38] Guo L, Xia Y, Jiao X, Chen D. *Ab initio* molecular dynamics study of the proton transfer in hydroxyl ion-induced hydrolysis of aluminum monomers. J Phys Chem B. 2023;127(33):7342–51. doi:10.1021/acs.jpcb.3c02805.
[39] L'Hôpital E, Lothenbach B, Le Saout G, Kulik D, Scrivener K. Incorporation of aluminium in calcium-silicate-hydrates. Cem Concr Res. 2015;75:91–103. doi:10.1016/j.cemconres.2015.04.007.
[40] Fu Q, Huang J. Structure of calcium silicate hydrate. Prog Mater Sci. 2026;159(9):101666. doi:10.1016/j.pmatsci.2026.101666.
[41] Myers RJ, Bernal SA, Gehman JD, van Deventer JSJ, Provis JL. The role of Al in cross-linking of alkali-activated slag cements. J Am Ceram Soc. 2015;98(3):996–1004. doi:10.1111/jace.13360.